Journal of Alloys and Compounds 505 (2010) 76–80

Contents lists available at ScienceDirect

Journal of Alloys and Compounds

journal homepage: www.elsevier.com/locate/jallcom

Precipitate-induced R-phase in martensitic transformation of as-spun and annealed $Ti_{51}Ni_{49}$ ribbons

Ling-Mei Wu [a], Shih-Hang Chang [b], Shyi-Kaan Wu [a,*]

[a] Department of Materials Science and Engineering, National Taiwan University, Taipei 106, Taiwan
[b] Department of Chemical and Materials Engineering, National I-Lan University, I-Lan 260, Taiwan

ARTICLE INFO

Article history:
Received 28 April 2010
Received in revised form 31 May 2010
Accepted 3 June 2010
Available online 11 June 2010

Keywords:
Metals and alloys
Rapid-solidification
Phase transitions
Shape memory
Transmission electron microscopy
TEM

ABSTRACT

Differential scanning calorimetry (DSC) results indicate that a two-step B2 → R → B19′ martensitic transformation and a one-step B19′ → B2 transformation exhibit in as-spun and in 200–600 °C annealed $Ti_{51}Ni_{49}$ ribbons. Guinier-Preston (GP) zones and Ti_2Ni precipitates are formed in ribbons annealed at ≦300 °C and ≧400 °C, respectively, and a conspicuous increase of DSC transformation peak temperature occurs in between 300 °C and 400 °C. The sizes of GP zones and Ti_2Ni precipitates increase with increased annealing temperature. Transmission electron microscope (TEM) observations show that GP zones can induce the R-phase and both of them are formed along $\langle 1\,0\,0\rangle_{B2}$ directions. DSC and TEM tests show that Ti_2Ni precipitates can induce the R-phase more than GP zones and the induced R-phase plates are also found along $\langle 1\,0\,0\rangle_{B2}$ directions. Experimental results show that the growing direction of R-phase plates is strongly confined by that of GP zones and Ti_2Ni precipitates. The length of R-phase plates can reach about 2 μm in 300 °C annealed ribbon.

1. Introduction

Recently, sputtered thin films and melt-spun ribbons of TiNi-based shape memory alloys (SMAs) have attracted much attention because of their potential application as microactuators [1–5]. The as-sputtered Ti-rich TiNi thin films are fully amorphous and need further crystallization. Guinier-Preston (GP) zones and Ti_2Ni precipitates are usually observed in Ti-rich thin films after annealing at temperatures above 450 °C [6–8]. The coherent stress fields developed around the plate-like GP zones are suggested to induce the R-phase in the martensitic transformation. This behavior is similar to the R-phase induced by the coherent stress fields around Ti_3Ni_4 precipitates in aged Ni-rich TiNi bulk SMAs [2,3,9–14]. In our previous studies, the as-spun $Ti_{51}Ni_{49}$ ribbons are essentially crystalline with abundant GP zones [15,16]. The size of the GP zones increases with the increase of annealing temperature up to 350 °C. But when the ribbon is annealed at temperatures above 350 °C, Ti_2Ni precipitates gradually form with the dissipation of GP zones. The $Ti_{51}Ni_{49}$ ribbons with GP zones exhibit a larger recoverable strain (with a maximum of 6.4% for 200 °C annealed ribbon) and a lower permanent strain (0.05% for 200 °C annealed ribbon) than those with Ti_2Ni precipitates. This characteristic comes from the fact that the twinning plates in the martensite can pass through the coherent stress fields around GP zones more easily than the semi-coherent stress fields around Ti_2Ni precipitates [2]. However, how these coherent or semi-coherent stress fields influence the formation of the R-phase in as-spun and annealed $Ti_{51}Ni_{49}$ ribbons has not yet been intensively studied. Thus, the aim of this study is to investigate the precipitation effect on the martensitic transformation behavior, especially on the formation of the R-phase for as-spun and annealed $Ti_{51}Ni_{49}$ ribbons.

2. Experimental procedures

$Ti_{51}Ni_{49}$ melt-spun ribbons were supplied by the Institute for Materials Research, Tohoku University, Japan, prepared using a single-roller melt-spinning technique. Detailed procedures regarding the fabrication of the melt-spun ribbons are described in Refs. [15,16]. The as-spun ribbon was 14 μm in thickness and 1.05 mm in width. Some of the as-spun ribbons were cut into several segments, sealed in quartz tubes, purged with argon gas and then annealed at 200 °C, 300 °C, 400 °C, 500 °C and 600 °C for 1 h followed by quenching in water. The martensitic transformation temperatures and the transformation enthalpies (ΔHs) of the as-spun and annealed $Ti_{51}Ni_{49}$ ribbons were determined by TA Q10 differential scanning calorimetry (DSC). The specimen weight used in the DSC test was about 2–4 mg and the heating/cooling rate was set as 10 °C/min. The microstructures of the as-spun and annealed $Ti_{51}Ni_{49}$ ribbons were observed and characterized at room temperature using a Philips-TECNAI G2 F20 transmission electron microscope (TEM) operated at 200 kV. The TEM specimens were prepared by an argon ion miller using G1 glue and a copper grid.

* Corresponding author at: Department of Materials Science and Engineering, National Taiwan University, 1, Roosevelt Rd., Sec. 4, Taipei 106, Taiwan.
Tel.: +886 2 23637846; fax: +886 2 23634562.
E-mail address: skw@ntu.edu.tw (S.-K. Wu).

0925-8388/$ – see front matter © 2010 Elsevier B.V. All rights reserved.
doi:10.1016/j.jallcom.2010.06.019

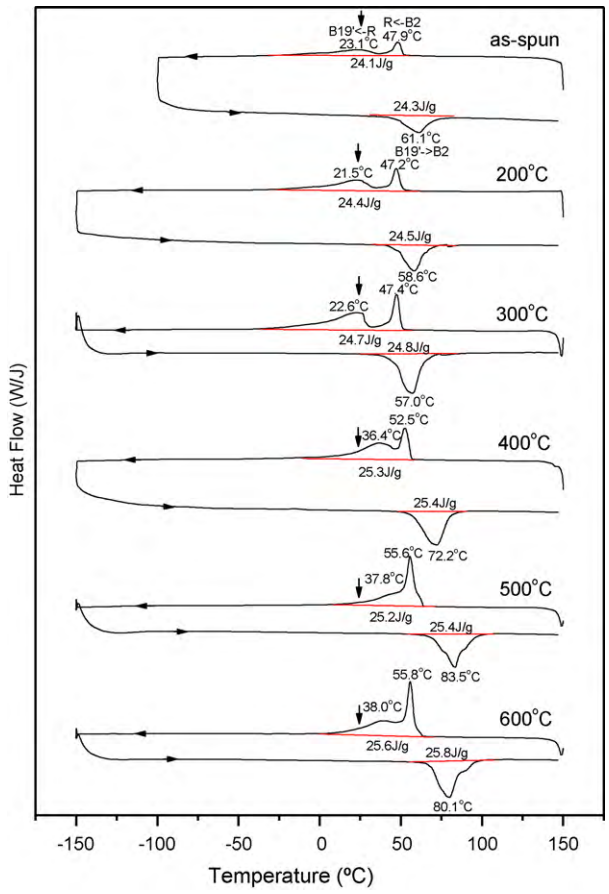

Fig. 1. DSC curves of the as-spun $Ti_{51}Ni_{49}$ ribbon and that annealed at 200 °C, 300 °C, 400 °C, 500 °C and 600 °C for 1 h. The arrow indicates the temperature is at 25 °C, i.e., the room temperature.

3. Results and discussion

3.1. DSC results

Fig. 1 shows the DSC cooling and heating curves of the as-spun $Ti_{51}Ni_{49}$ ribbon and the ribbons annealed at 200–600 °C for 1 h. Fig. 1 shows that each specimen exhibits a two-stage B2 → R → B19′ martensitic transformation in cooling but has only a one-stage B19′ → B2 transformation in heating. For ribbons annealed at temperatures above 400 °C, as shown in Fig. 1, the B2 → R and R → B19′ transformation peaks gradually come closer to each other with increased annealing temperature. Fig. 1 also reveals that all the ΔH values associated with martensitic transformation for as-spun and annealed ribbons are about 24–25 J/g. These values are close to that of bulk $Ti_{50}Ni_{50}$ SMA (typical about 25 J/g), which indicates that the as-spun $Ti_{51}Ni_{49}$ ribbon is already fully crystallized [15]. At the same time, as shown in Fig. 1, the peak temperatures of B2 → R and R → B19′ transformations increase significantly from 47.9 °C to 55.8 °C and from 23.1 °C to 38.0 °C, respectively. With the increased annealing temperature, there is an especially noticeable increment at the temperature between the annealing temperature of 300 °C and 400 °C. This is because the higher annealing temperature can eliminate more residual stress and defects originating from the melt-spinning process and they can depress the martensitic transformation. This feature can also be attributed to the different precipitates formed in the annealed ribbons, i.e. the precipitates are gradually changed from GP zones to Ti_2Ni, together with an alternation of stress fields around them, as the annealing temperature is between 300 °C and 400 °C.

3.2. TEM observations

Fig. 2(a) shows a bright field (BF) image of the as-spun $Ti_{51}Ni_{49}$ ribbon and the corresponding selected area diffraction patterns (SADP) along the $[1\,0\,0]_{B2}$ zone axis. From the SADP shown in Fig. 2(a), diffraction spots of the R-phase are observed at 1/3 positions along $[0\,1\,1]^*_{B2}$ and $[0\,1\,\bar{1}]^*_{B2}$. Formation of the R-phase at room temperature can be further confirmed by the DSC cooling curve of Fig. 1 for as-spun ribbons because its B2 → R transformation peak appears at a temperature higher than room temperature. From Fig. 2(a), transformed R-phase variants are found to develop along two different $\langle 0\,1\,0\rangle_{B2}$ directions in as-spun ribbons, as indicated by arrows. With the exception of the 1/3 spots along $[0\,1\,1]^*_{B2}$ and $[0\,1\,\bar{1}]^*_{B2}$, Fig. 2(a) shows there are some other 1/3 spots with lower intensity, originating from the double diffraction. Fig. 2(b) shows a magnification of Fig. 2(a), illustrating the GP zones more clearly in which the GP zones, as indicated by the arrows, are about 7 nm long. Fig. 2(b) also shows many dislocations in the matrix, as indicated by the double arrows.

Fig. 3(a) shows the BF image of the ribbon annealed at 200 °C for 1 h and the corresponding SADP along the $[1\,0\,0]_{B2}$ zone axis. Fig. 3(a) reveals that the long straight plates of the R-phase are mainly along the $[0\,1\,0]_{B2}$ direction. Fig. 3(b) shows a magnification of Fig. 3(a) depicting that most of the GP zones in the ribbon are also along the $[0\,1\,0]_{B2}$ direction and their average length increases to

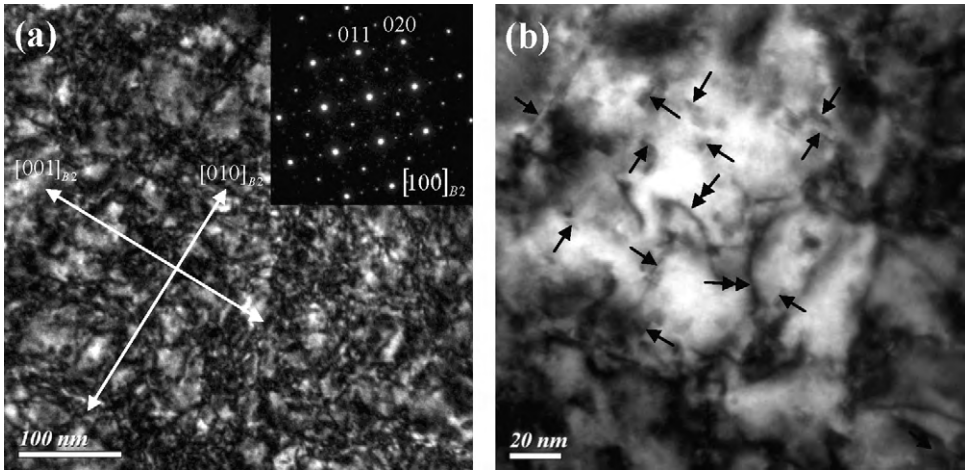

Fig. 2. (a) Bright field image of the as-spun ribbon and the SADP observed along the [100] zone axis. (b) Magnification of (a).

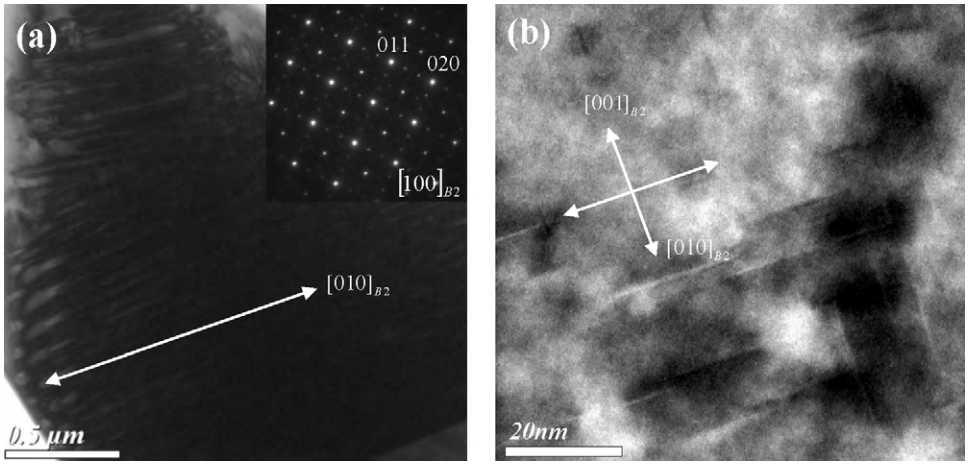

Fig. 3. (a) Bright field image of the $Ti_{51}Ni_{49}$ ribbon annealed at 200 °C for 1 h and the SADP observed along the $[1\,0\,0]_{B2}$ zone axis. (b) Magnification of (a).

about 20 nm after 200 °C annealing. Fig. 3(a and b) demonstrates that the growth orientation of the R-phase plates is identical to that of the existing GP zones. This characteristic implicates that the growing directions of R-phase variants are strongly confined by those of plate-like GP zones that are formed along $\langle 0\,1\,0\rangle_{B2}$ directions of $\{1\,0\,0\}_{B2}$ planes [8,15]. Fig. 4(a) shows a BF image of the $Ti_{51}Ni_{49}$ ribbon annealed at 300 °C for 1 h, revealing that the R-phase plates can extend to about 2 μm in length and there are several subgrains formed in the original B2 grain. Fig. 4(b and c) shows magnifications of Fig. 4(a) and the corresponding SADPs taken along the $[1\,0\,0]_{B2}$ zone axis marked at A and B, respectively. Fig. 4(b and c) indicates that in each subgrain the R-phase plates have the same $\langle 0\,1\,0\rangle_{B2}$ direction as the existing GP zones, a behavior similar to the example illustrated in Fig. 3(a and b). However, the GP zones cannot be observed in Fig. 4 because they are shielded by the R-phase plates.

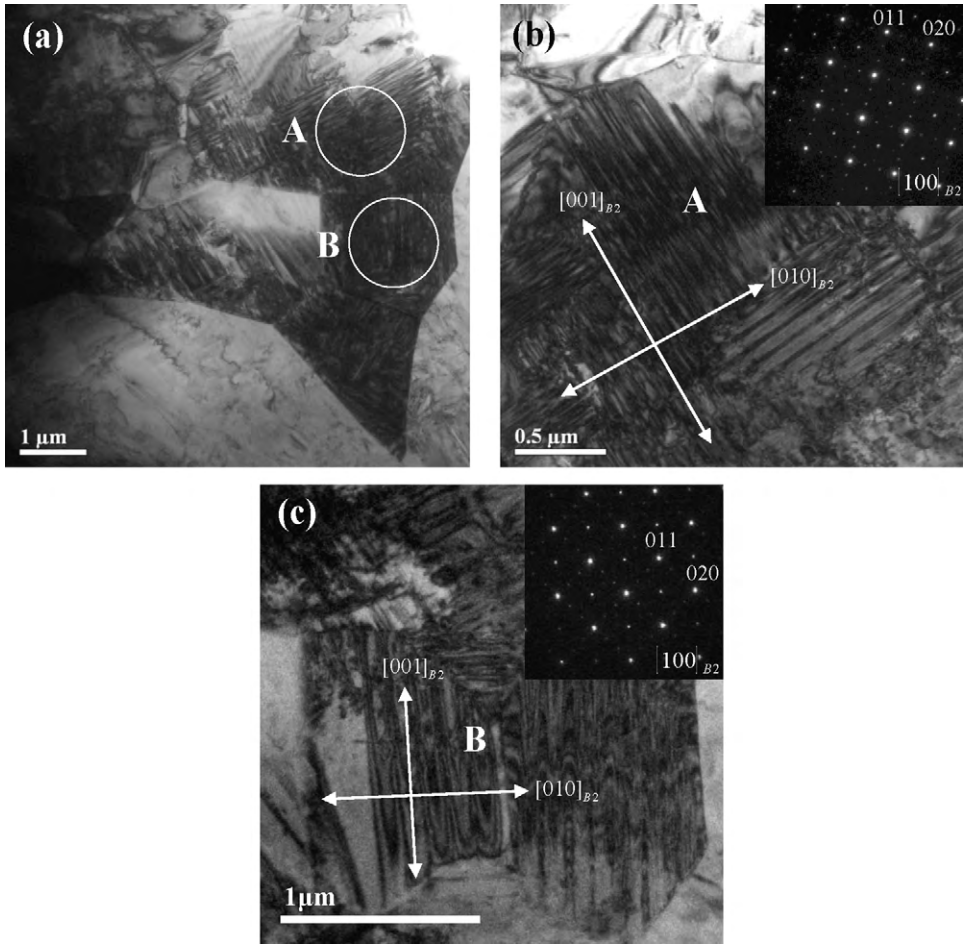

Fig. 4. (a) Bright field image of the $Ti_{51}Ni_{49}$ ribbon annealed at 300 °C for 1 h and the SADP along $[1\,0\,0]_{B2}$ zone axis and the magnification of the areas marked at (b) A and at (c) B.

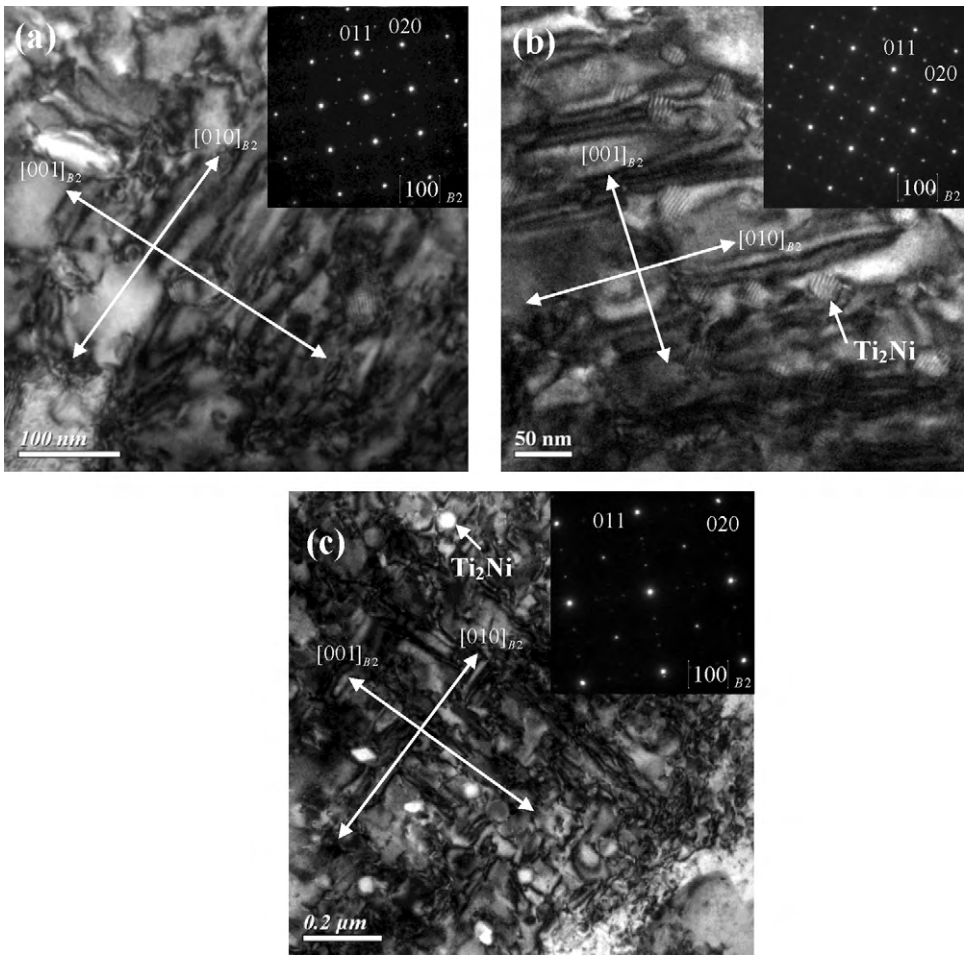

Fig. 5. Bright field images of the $Ti_{51}Ni_{49}$ ribbons annealed at (a) 400 °C, (b) 500 °C, and (c) 600 °C for 1 h with their SADP results along $[1\,0\,0]_{B2}$ zone axis.

Fig. 5(a–c) shows the TEM BF images and the corresponding SADPs taken along the $[1\,0\,0]_{B2}$ zone axis of $Ti_{51}Ni_{49}$ ribbons annealed at 400 °C, 500 °C and 600 °C for 1 h, respectively. Fig. 5 shows that the GP zones disappear and only nanosize Ti_2Ni precipitates with Moiré fringes can be observed, as indicated by arrows. This is because the formation of Ti_2Ni precipitates accompanies the dissipation of the GP zones [16]. The DSC results shown in Fig. 1 indicate that the B2 → R transformation peak of $Ti_{51}Ni_{49}$ ribbons annealed at 400–600 °C × 1 h is as significant as that of the ribbons annealed at 200–300 °C × 1 h. This characteristic indicates that the semi-coherent stress fields around Ti_2Ni precipitates can effectively induce R-phase in the martensitic transformation. However, Fig. 5 reveals that the long R-phase plates shown in Fig. 3(a) no longer exist, and instead only short R-phase plates linger, which are also along the $[0\,1\,0]_{B2}$ and $[0\,0\,1]_{B2}$ directions.

3.3. Discussion on the R-phase formation in the martensitic transformation of as-spun and annealed $Ti_{51}Ni_{49}$ ribbons

3.3.1. Effect of GP zones in as-spun and 200 °C/300 °C annealed ribbons

From TEM observations of as-spun and 200 °C/300 °C annealed ribbons, the growing orientations of the transformed R-phase plates are along the $\langle 1\,0\,0\rangle_{B2}$ directions, as are those of the existent plate-like GP zones that are formed on $\{1\,0\,0\}_{B2}$ planes of the B2 matrix. This characteristic may imply that the largest coherent stress fields around the GP zones are along $\langle 1\,0\,0\rangle_{B2}$ directions of $\{1\,0\,0\}_{B2}$ planes and the R-phase plates are confined to form along $\langle 1\,0\,0\rangle_{B2}$ directions. For as-spun and 200 °C/300 °C annealed ribbons, both the lengths of the GP zones and the transformed R-phase plates increase with increased annealing temperature. This indicates that with longer GP zones, the volume of coherent stress fields around GP zones is higher, and there is more precipitation effect of GP zones on the growing length of R-phase plates. From Fig. 4, the length of R-phase plates can reach about 2 μm. At the same time, there are several subgrains formed in the original B2 grain of Fig. 4(a) and each subgrain has its individual $\langle 1\,0\,0\rangle_{B2}$ direction for the R-phase plates. This characteristic can be understood from Fig. 3(b), where there are more precipitates of the GP zones along the $[0\,1\,0]_{B2}$ direction than along the $[0\,0\,1]_{B2}$ direction. Therefore, the induced R-phase plates are mainly along the $[0\,1\,0]_{B2}$ direction, instead of the $[0\,0\,1]_{B2}$ direction, as shown in Fig. 3(a).

3.3.2. Effect of Ti_2Ni precipitates in 400–600 °C annealed ribbons

TEM observations of $Ti_{51}Ni_{49}$ ribbons annealed at 400–600 °C demonstrate that nanosize disc-like Ti_2Ni precipitates are formed instead of GP zones. According to the DSC results of Fig. 1, the peak temperatures of B2 → R and R → B19′ transformations show a conspicuous increase between the annealing temperature of 300 °C and 400 °C. This is because the precipitates formed in annealing ribbons change gradually from GP zones to Ti_2Ni in this temperature range, as mentioned in Section 3.2. DSC results also indicate that the B2 → R transformation peak is more significant for the ribbons annealed at 400–600 °C than those annealed at 200–300 °C. As demonstrated in Section 3.2, we propose that the semi-coherent stress fields around Ti_2Ni precipitates can effectively induce the

R-phase, similar to those coherent stress fields around GP zones. However, the more significant B2 → R transformation peak appearing in the DSC cooling curve of 400–600 °C annealed ribbons comes from the fact that the precipitate size of Ti_2Ni is much larger than that of GP zones. The diameter of Ti_2Ni precipitates is 5–15 μm for ribbons annealed at 350 °C × 1 h and it can reach about 50 μm for ribbon annealed at 600 °C × 1 h [16]. The growing size of Ti_2Ni precipitates increases the volume of the semi-coherent stress fields around them and induces more transformed R-phase plates. This feature can be also observed from the increased DSC peak height of B2 → R transformation as the annealing temperature increases from 400 °C to 600 °C. As to the R-phase plates, TEM observations indicate that the R-phase plates in ribbons annealed at 400–600 °C are much shorter than those annealed at 200–300 °C. This is because Ti_2Ni precipitates can not only hinder the shear deformation of martensitic transformation [2], but also impede the growth of R-phase plates. The nanosize disc-like Ti_2Ni precipitates grow on $\{1\,0\,0\}_{B2}$ planes and have an orientation relationship of $(1\,0\,0)_{B2}//(0\,0\,4)_{TiNi}$ and $[0\,1\,1]_{B2}//(0\,4\,4)_{TiNi}$ with the B2 matrix [6,16]. The reported lattice constants of TiNi B2 and Ti_2Ni phases are 0.301 nm [17] and 1.131 nm [18,19], respectively. From this orientation relationship, the lattice misfit along $\langle 1\,0\,0\rangle_{B2}$ directions of $\{1\,0\,0\}_{B2}$ planes is about 6.1%. From Fig. 5, the growing directions of R-phase plates in ribbons annealed at 400–600 °C are also along $\langle 0\,1\,0\rangle_{B2}$ directions, similar to those induced by GP zones, as shown in Figs. 2–4. This may imply that the Ti_2Ni precipitates have their maximal stress fields along $\langle 0\,1\,0\rangle_{B2}$ directions of the $\{0\,1\,0\}_{B2}$ planes. Therefore, from Figs. 2–5, the growing orientation of the R-phase plates is strongly confined by that of GP zones and Ti_2Ni precipitates.

4. Conclusions

The as-spun $Ti_{51}Ni_{49}$ ribbon has many GP zones and their size gradually increases with increased annealing temperature. The precipitations in the annealed ribbons are gradually changed from GP zones to Ti_2Ni when the annealing temperature is increased from 300 °C to 400 °C. This causes a significant increase of B2 → R and R → B19′ DSC transformation peak temperatures. Plate-like GP zones are formed along $\langle 1\,0\,0\rangle_{B2}$ directions of $\{1\,0\,0\}_{B2}$ planes and TEM observations show that R-phase plates are also formed along $\langle 1\,0\,0\rangle_{B2}$ directions. Nanosize disc-like Ti_2Ni precipitates with semi-coherent stress fields around them are formed in ribbons when annealed at 400–600 °C. The orientation relationship of Ti_2Ni precipitates and the B2 matrix is $(1\,0\,0)_{B2}//(0\,0\,4)_{TiNi}$ and $[0\,1\,1]_{B2}//\langle 0\,4\,4\rangle_{TiNi}$ in which the lattice misfit is calculated as about 6.1% in the $\langle 1\,0\,0\rangle_{B2}$ directions. TEM observations indicate that the R-phase formation induced by Ti_2Ni precipitates is also along $\langle 1\,0\,0\rangle_{B2}$ directions. The growing directions of the R-phase induced by GP zones and Ti_2Ni precipitates are clearly all along $\langle 1\,0\,0\rangle_{B2}$ directions and are suggested to be strongly confined by the largest stress fields around the GP zones and Ti_2Ni precipitates.

Acknowledgement

The authors gratefully acknowledge the financial support for this research from the National Science Council (NSC), Taiwan, Republic of China, under the Grant NSC97-2221-E002-035-MY3.

References

[1] S. Miyazaki, A. Ishida, Mater. Sci. Eng. A 273–275 (1999) 106–133.
[2] J.X. Zhang, M. Sato, A. Ishida, Acta Mater. 51 (2003) 3121–3130.
[3] M. Tomozawa, H.Y. Kim, S. Miyazaki, Acta Mater. 57 (2009) 441–452.
[4] H. Rösner, P. Schloβmacher, A.V. Shelyakov, A.M. Glezer, Acta Mater. 49 (2001) 1541–1548.
[5] T.H. Nam, J.H. Lee, D.W. Jung, C.A. Yu, Y. Liu, Y.W. Kim, Mater. Sci. Eng. A 449–451 (2007) 1041–1044.
[6] A. Ishida, K. Ogawa, M. Sato, S. Miyazaki, Metall. Mater. Trans. A 28 (1997) 1985–1991.
[7] T. Kikuchi, K. Ogawa, S. Kajiwara, T. Matsunaga, S. Miyazaki, Y. Tomota, Phil. Mag. A 78 (1998) 467–489.
[8] J.X. Zhang, M. Sato, A. Ishida, Acta Mater. 49 (2001) 3001–3010.
[9] S. Kajiwara, T. Kikuchi, K. Ogawa, T. Matsunaga, S. Miyazaki, Phil. Mag. Lett. 74 (1996) 137–144.
[10] A. Ishida, M. Sato, T. Kimura, T. Sawaguchi, Mater. Trans. JIM 42 (2001) 1060–1067.
[11] T. Yamamoto, H. Kato, Y. Murakami, H. Kimura, A. Inoue, Acta Mater. 56 (2008) 5927–5937.
[12] S.K. Wu, H.C. Lin, T.S. Chou, Acta Metall. Mater. 38 (1990) 95–102.
[13] L. Hou, D.S. Grummon, Scripta Metall. Mater. 33 (1995) 989–995.
[14] A. Ishida, A. Takei, M. Sato, S. Miyazaki, Thin Solid Films 281–282 (1996) 337–339.
[15] S.H. Chang, S.K. Wu, L.M. Wu, Intermetallics 18 (2010) 965–971.
[16] L.M. Wu, S.K. Wu, Phil. Mag. Lett. 90 (2010) 261–268.
[17] P. Villars, L.D. Calvert (Eds.), Pearson's Handbook of Crystallographic Data for Intermetallic Phases, 2nd ed., ASM International, Materials Park, Ohio, 1991, p. 44073.
[18] JCPDS, International Center for Diffraction Data, 05-0687, 1997.
[19] F.M. Miller, Chemistry: Structures and Dynamics, McGraw-Hill, New York, 1984.